Advanced Composite Materials
Publication details, including instructions for authors and subscription information:
http://www.tandfonline.com/loi/tacm20

Experimental investigation on thermochemical phenomena in SiFRP

Kenichi Hirai [a], Yoshiki Matsuura [a], Kiyoshi Kinefuchi [b] & Toru Kamita [b]

[a] IHI Aerospace Co., Ltd, Technologies Development Department, Fujiki 900, Tomioka-shi, Gunma, 370-2307, Japan

[b] Japan Aerospace Exploration Agency, 2-1-1 Sengen, Tsukuba-shi, Ibaraki, 305-8505, Japan

Version of record first published: 19 Nov 2012.

To cite this article: Kenichi Hirai , Yoshiki Matsuura , Kiyoshi Kinefuchi & Toru Kamita (2012): Experimental investigation on thermochemical phenomena in SiFRP, Advanced Composite Materials, 21:5-6, 459-475

To link to this article: http://dx.doi.org/10.1080/09243046.2012.743715

Advanced Composite Materials
Vol. 21, Nos. 5–6, October–December 2012, 459–475

Experimental investigation on thermochemical phenomena in SiFRP

Kenichi Hirai[a]*, Yoshiki Matsuura[a], Kiyoshi Kinefuchi[b] and Toru Kamita[b]

[a]*IHI Aerospace Co., Ltd, Technologies Development Department, Fujiki 900, Tomioka-shi, Gunma 370-2307, Japan;* [b]*Japan Aerospace Exploration Agency, 2-1-1 Sengen, Tsukuba-shi, Ibaraki 305-8505, Japan*

(*Received 8 May 2012; final version received 26 June 2012*)

This study focuses on understanding and modeling the physical phenomena that occur in degraded zones of silica-phenolic (SiFRP) materials under exposure to high-temperature gasses when applied to a liquid rocket engine (LRE) combustor. Although understanding and modeling these phenomena is considered essential in designing an LRE combustor, few studies on these fields can be found in the available literature. Basically, it is well known that when ablators are heated, a pyrolysis reaction proceeds in them, forming three distinct zones: a charred, a decomposed, and a virgin zone. The obtainable information for the thermal response of SiFRP in ground-firing tests is classified in two categories. The first category involves the equilibrium state characteristics after a long time has elapsed following burnout. This refers to the degraded thickness distribution, which reflects 3D information (the combustor's inner surface x the thickness direction) regarding the heat load distribution over the entire combustor's inner surface, owing to the highly insulating nature of SiFRP. The second category involves the transient characteristics of the propagation of the degraded zones in SiFRP, which can be detected using an ultrasonic testing (UT) method. In this paper, the progress of in-depth phenomena of SiFRP and their physical variations were intentionally studied. Our aim was to clarify and specify the quantitative threshold values of the interface points that characterize each degraded zone and the UT reflection point, and then express these values in terms of physical quantities that could appear in a numerical analysis.

Keywords: ablation; heat shield; liquid rocket engine; surface recession; silica phenolic

1. Introduction

The silica-phenolic (SiFRP) material studied in this paper was manufactured by IHI Aerospace Co., Ltd. The SiFRP material was fabricated by curing a prepreg, which consists of phenolic resin-impregnated multiple stacked fabrics made of SiO_2 continuous fibers. The SiO_2 fibers used in SiFRP consist of high-purity materials whose purity exceeds 99%. Thus, when the SiFRP material is heated, it goes through multiple stages of pyrolysis reactions within the phenolic resin until a charred zone of a carbon and SiO_2 mixture eventually appears. A liquid rocket engine (LRE) that is currently being produced adopts SiFRP as a material for the heat shield of its combustor.

In this paper, we focus on a specific type of LRE, in which cryogenic propellants such as liquefied oxygen (LOX) and liquefied natural gas (LNG) are adopted. For most of the duration

*Corresponding author. Email: kenichi-h@iac.ihi.co.jp

ISSN 0924-3046 print/ISSN 1568-5519 online

http://dx.doi.org/10.1080/09243046.2012.743715
http://www.tandfonline.com

of the engine's operation, these propellants are in a liquid state when they are injected into the combustor. In the present injector, as the fuel flow is injected through the multiple holes located in the outermost section of the injector faceplate, the injected fuel flows along the combustor's inner surface, providing the so-called film cooling effect on these surfaces. As schematically shown in Figure 1, a mixing layer may be formed in the intermediate zone between the core combustion gasses and the combustor's inner surfaces, which consists of a film cooling layer and a pyrolysis gas layer.

The convective heat flux ($\dot{q}_{conv}$) on the combustor's inner surfaces is generally expressed by Equation (1), where h is the heat transfer coefficient, T_w is the combustor's wall temperature, and T_g is the effective combustor gas temperature. T_g is considered to be the gas temperature adjacent to the combustor wall, which is under the influence of the film cooling effect.

$$\dot{q}_{conv} = h \times (T_g - T_w) \tag{1}$$

Here, T_g is expected to be much lower than the effective gas temperature in the core flow (T_{ad}), which is calculated using Equation (2), where T_{ad} is the adiabatic combustion temperature, and η is the energy release efficiency of the LRE.

$$T_{eq} = T_{ad} \times \eta^2 \tag{2}$$

The physical phenomena appearing in the LRE are quite complex, as shown in the examples below.

(1) In the core zone of the LRE.

Here, liquid phase vaporization, 3D (dimensional) mixing between the fuel and the oxidizer, and combustion (chemical reaction) occur.

(2) In the peripheral zone of the LRE.

(2–1) Film Coolant

The liquid phase vaporization, mixing, and chemical reactions with the core flow.

(2–2) Pyrolysis gasses from SiFRP.

The injection of pyrolysis gasses and mixing with chamber gasses.

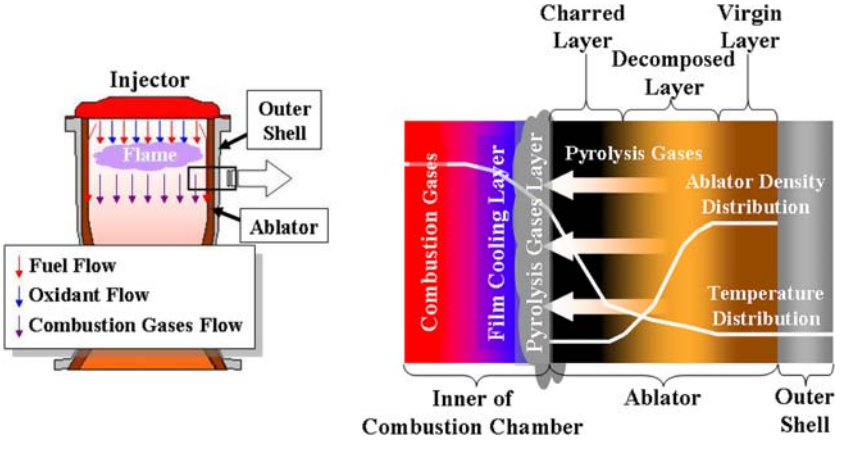

Figure 1. Image of film cooling and ablative cooling in a liquid rocket engine.

Owing to these complex physical phenomena within the actual combustor, reliable quantitative prediction of the convective heat load or gas temperature distribution presents a very challenging task, even with the help of the latest CFD (computational fluid dynamics) technologies.

On the other hand, published papers [1,2] have reported that a number of researchers have conducted heat flux estimations of the combustor's inner surface in two different ways.

(1) Using a water-cooled engine.
This was done by installing a set of annular water cooling pipes made of Cu around the combustor, along which the axial heat flux distribution could be evaluated in terms of the coolant (water) flow rate and the rise in coolant temperature for each cooling pipe.
(2) Using a radiation-cooled engine.
This was done using a special refractory metal, such as a Columbium alloy combustion chamber, which makes it possible to determine the average heat flux on the wall, as given by radiation thermometers.

With regard to (1), owing to the restrictions imposed by the test facilities, annular water cooling techniques can be applied only to small-sized engines and cannot be applied to larger engines. With regard to (2), the use of Columbium alloy is problematic in Japan because both the oxidation resistance coating process and machining process must be outsourced to the USA.

For this reason, the authors have come to adopt a strategy in which the environmental heating conditions during LRE ground-firing tests are determined inversely to account for the measured degraded thicknesses [3,4], taking advantage of the highly insulating nature of SiFRP. Here, the degraded thickness is the sum of the thicknesses of the charred zone and the decomposed zone formed inside SiFRP during and after heating. The environmental heating conditions imply the value of T_g that appears in Equation (1).

In employing this strategy, we consider that the following conditions must be met.

(a) The characteristics defining the interface points that divide the charred, decomposed, and virgin zones should be clarified and quantified (see Section 2.2).
(b) The numerical model for determining the SiFRP thermal response should be verified and validated under well-defined boundary conditions.

Next, we present a detailed explanation regarding these essential points.

The degraded thickness obtained after ground-firing tests can be viewed as a useful measure because it reflects 2D information regarding the heat load distribution over the entire combustor's inner surface, owing to the highly insulating nature of ablators.

Therefore, we think it is safe to say that the data obtained for the degraded zones in firing tests will contain 3D information (the combustor's inner surface × thickness-direction) that is both visual and comprehensive. This result is superior to the results of in-depth temperature measurements, which could provide only restricted and local information because they were limited in terms of both number and locations.

The degraded thickness could be easily determined by our own eyes and with the use of vernier calipers. Here, it is important to relate these measured quantities to the quantities obtainable via computation. In addition, we must admit that this measured 3D information would still be limited because it only provides information about the equilibrium state long after burnout, and thus does not include transient characteristics. Usually, the thickness of an ablative combustor is designed such that the decomposed zone does not reach the metal outer shell, and such that the adhesive temperature between the SiFRP material and the shell is less than the maximum allowable temperature for the applied adhesive before the designated time has elapsed. Therefore, we need to accurately predict the in-depth temperature and

evolvement of the degraded zone. These predictions should be made based not only on the measured equilibrium values (the thickness of the degraded zones), but also on the reliable transient thermal analysis that covers the period from the initial state to the designated elapsed time. Thus, while predicting the thermal behavior of a SiFRP combustor of an LRE, a knowledge of the equilibrium characteristics such as the thickness of the degraded zones are required. In addition, a knowledge of the transient characteristics such as propagation of the degraded zones based on measurements using ultrasonic testing (UT) techniques or in-depth temperatures are required. Here, with regard to the use of UT techniques, it is also indispensible to determine the UT reflection characteristics.

In this research, upon characterizing the SiFRP in-depth phenomena, we begin classifying the distinct zones that appear inside SiFRP after heating tests are carried out, as shown in Figure 2. They are:

(1) Charred Zone.
(2) Decomposed Zone.
(3) Virgin Zone.

The same qualitative classifications can be found in a 2007 review paper [5] by Joseph Koo of Texas University (see also Figure 3), though the quantitative investigation results

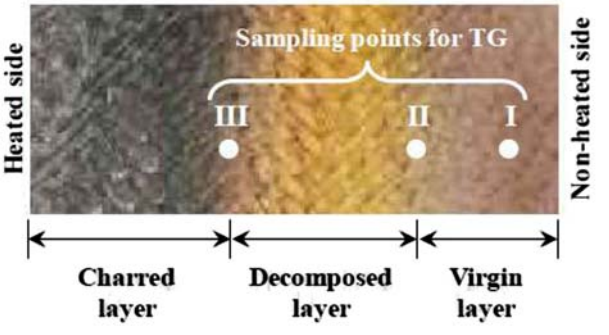

Figure 2. Appearance of ablator after heating test and TG sampling points.

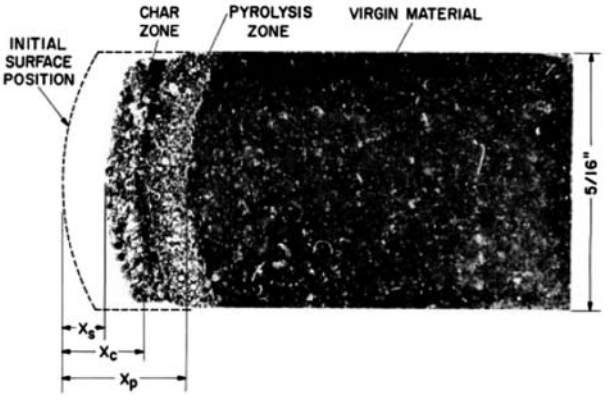

Figure 3. Post-run condition of arcjet test specimen [5].

are apparently not available to the public. Likewise, in a recent paper [2], researchers at Aerojet also made comparisons between the computed and the measured degraded thickness, but their definitions of the degraded zones are not presented.

Thus, we have come to believe that research activities in the characterization and modeling of SiFRP phenomena in depth are not only essential for the thermal design of an ablative-cooled LRE, but it would also provide new research findings just like those on SiFRP surface phenomena [6].

This is precisely why we have decided to direct our research toward 'experimental investigations on thermochemical phenomena in SiFRP.'

In the following sections, we relate the above-mentioned two interface (I/F) points to the quantities that can be obtained as a result of numerical computation, such as the extent of the pyrolysis reaction (β) or the maximum experienced temperature (MET).

2. Characterization of degraded zones using TG-based approach

2.1. Outline for experiments

To understand the physical meaning of the degraded zones formed inside SiFRP, we took samples for conducting thermogravimetry (TG) tests from SiFRP combustors after firing tests at multiple axis locations along the combustor axis, as well as at multiple angle locations around the axis. At each location, we took samples of approximately 20 mg from each of the two I/F points (denoted as III and II in Figure 2**)** and one from the virgin zone (I). The samples were placed inside the oven of the TG equipment and heated to 1100 °C, at which point the pyrolysis reactions were almost complete under an argon atmosphere at a heating rate of 10 °C/min. By comparing the mass loss data at points II and III to the data at point I, we could easily determine the extent of the pyrolysis reactions at II and III that the phenolic resin underwent during heating. Upon sampling, 0.75-mm-diameter diamond drills were used for both II and III, whereas a 1.50-mm-diameter drill was used for I. Here, I, II, and III represent the following:

Point I: Virgin zone.
Point II: I/F of decomposed and virgin zones.
Point III: I/F of charred and decomposed zones.

2.2. Analysis of measurement results

Here, the extent of the pyrolysis reactions (β) is defined by Equation (3), where the initial weight is W_0, the final weight is W_f, and the weight at an arbitrary time t is $W(t)$.

$$\beta = \frac{W_0 - W(t)}{W_0 - W_f} \tag{3}$$

Data analysis after the TG tests was performed using the following procedures:

(a) Step one: obtain the TG data at point I.
(b) Step two: obtain the TG data at points II and III.
(c) Step three: estimate the β values at points II and III by comparisons with (a) and (b).

An example of the TG data obtained is shown in Figure 4.

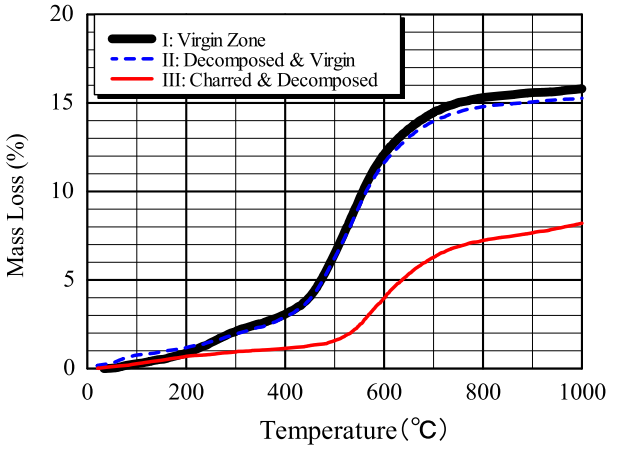

(a) Raw Data

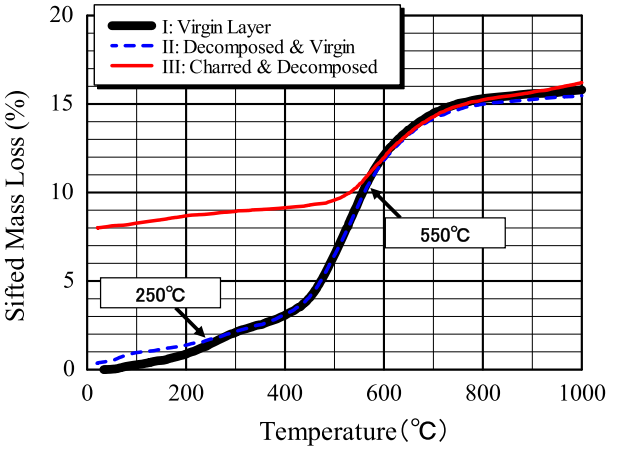

(b) Sifted from Raw Data

Figure 4. TG data for heated SiFRP specimen.

First, in Figure 4(a), we can observe that the TG data for II look similar to that for I, and it is then estimated that the process from I to II is not accompanied by any changes in weight. Thus, we can conclude that II cannot be characterized by the TG data or by β.

In contrast to II, the TG data for III look much different from the data for I, and it is then estimated that the process from II to III is accompanied by a significant weight loss. Figure 4 (b) is a version of Figure 4(a) that has been modified so that there is overlapping in the higher temperature region (higher than 600 °C). In Figure 4(b), it appears that II branches from I at around 250 °C and III branches from I at around 550 °C. We can therefore conclude that the MET for II is determined to be 250 °C and the MET for III is 550 °C.

On the other hand, the mass loss rate (R) is expressed in Equation (4), where the sample weight is m, the time is t, and the temperature is T. The R is expected to be proportional to the temperature derivative of the weight ($\mathrm{d}m/\mathrm{d}T$). An example of the results of the TG derivative is shown in Figure 5. In this figure, the integral value with respect to T up to a specified temperature indicates the total mass loss up to that temperature.

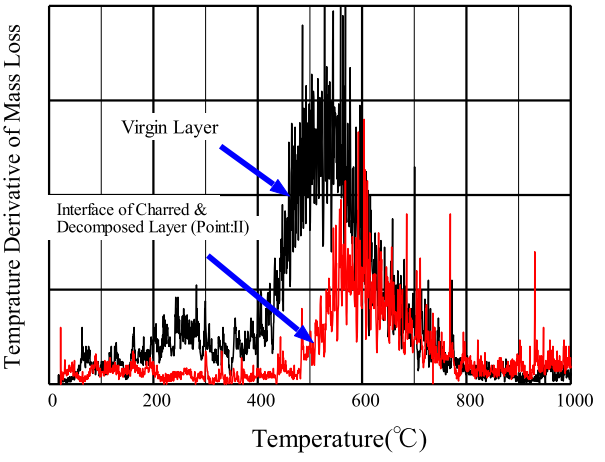

Figure 5. Temperature derivative of TG data for heated SiFRP specimen.

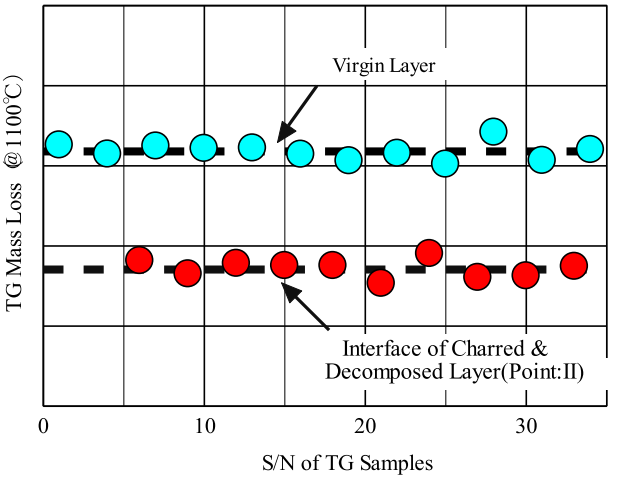

Figure 6. Comparison of TG mass loss at 1100 °C for I and III.

$$R = \frac{1}{m_0}\frac{\mathrm{d}m}{\mathrm{d}t} = \frac{1}{m_0}\frac{\mathrm{d}m}{\mathrm{d}T}\frac{\mathrm{d}T}{\mathrm{d}t} \propto \frac{1}{m_0}\frac{\mathrm{d}m}{\mathrm{d}T} \tag{4}$$

In Figure 5, we notice that the TG derivative at III is almost zero up to 500 °C, which means that the reaction up to around 500 °C is almost complete in the charred zone. We also noticed that it overlaps with the derivative at I in the temperature region that exceeds 600 °C. Thus, the temperature corresponding to III lies between 500 and 600 °C, and III also seems to correspond to the peak temperature of the pyrolysis reactions. Also, with the help of Figure 4(b), we can confirm that the β value at III (β_{III}) can be estimated at approximately 40%.

Furthermore, a summary of the mass loss data for III up to 1100 °C is presented in Figure 6. The horizontal axis (=X) stands for the ID number of the specimens. From these procedures, we are finally able to confirm the validity of $\beta_{\mathrm{III}} \cong 40\%$.

3. Characterization of degraded zones in halogen lamp Experiments

3.1. Outline of experiments

As shown in Figure 4, because II branches from I at 250 °C with no mass loss, it seems difficult to characterize II in terms of the extent of the pyrolysis reactions. Our idea for addressing this, then, is as follows:

(a) Step one: conduct heating tests using a 50 mm (D) × 25 mm (H) cylindrical SiFRP specimen with multiple thermocouple (T/C) measurements in the depth direction.
(b) Step two: measure the depth of II after the tests.
(c) Step three: estimate the MET at II by correlating the maximum temperature at each T/C and the relative distance between the depths of II with respect to each T/C position.

As heating equipment, we used a halogen lamp (Fintech Co. Ltd, HSH-160/100 V-2 kW, exit diameter 160 mm, 160 V × 20 A) that can deliver a maximum heat flux of 350 kW/m^2 for a 50-mm-diameter specimen by concentrating the light with the help of a gold-coated mirror. The actual heat flux was determined using a Medtherm Co. Ltd heat flux sensor, and we obtained the correlation between the supply voltage and the specimen distance from the halogen lamp. A photograph of the halogen lamp test setup is shown in Figure 7.

3.2. Basic idea for data analysis

Figure 8 shows a schematic representation of the test specimen. The K-type T/Cs were installed at depths of 3, 6, and 10 mm from the heated surface inside each test specimen to monitor the temperature responses. The heating rate ranged from 100 to 300 kW/m^2 depending on the test. The heating time was fixed at seconds. After each test, the charred and decomposed thicknesses were measured using vernier calipers and our own eyes. For example, when the penetration depth of the decomposed zone reached 4 mm, the MET for II was

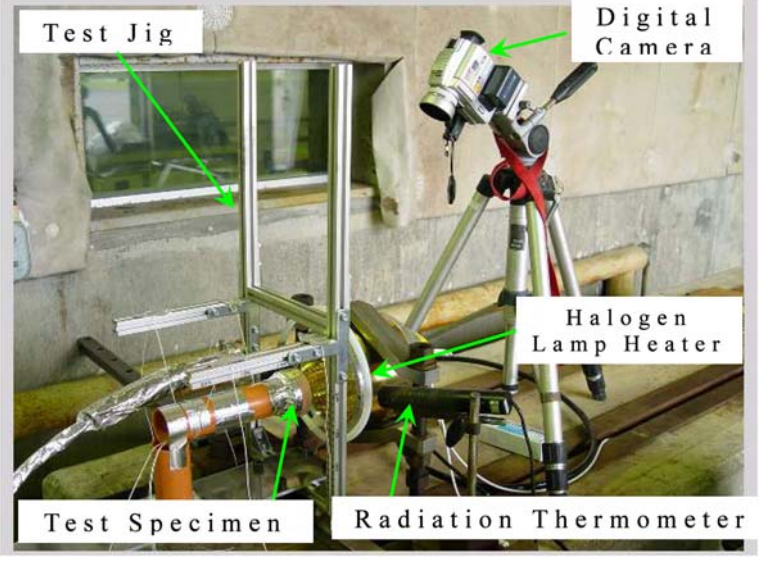

Figure 7. Photograph of halogen lamp test setup.

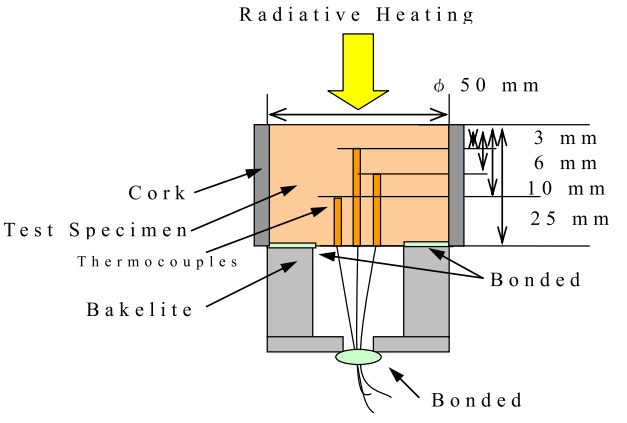

Figure 8. Diagram of halogen lamp test specimen.

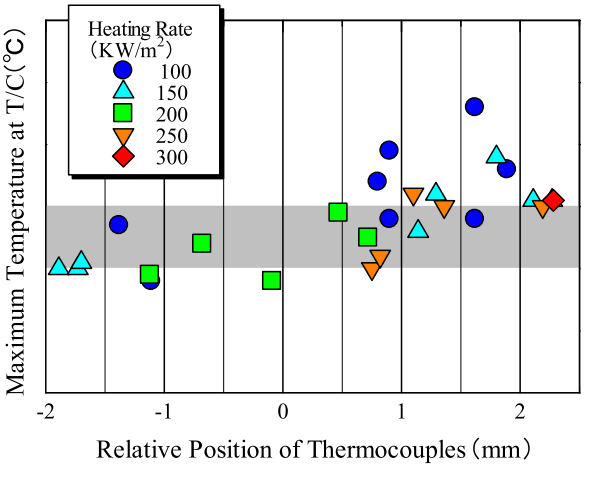

Figure 9. Experimental correlation between maximum temperature and relative position of thermocouples obtained from halogen lamp test.

estimated using both the 3-mm-depth T/C and the 6-mm-depth T/C, even though this produced a very rough estimate.

3.3. Analysis of measurements results

The obtained correlation data are shown in Figure 9, where X corresponds to the relative location of each T/C, i.e the penetration depth of the decomposed zone minus the T/C position, and Y corresponds to the MET for each T/C. From Figure 9, we can confirm that the MET for II (T_{II}) is slightly less than 250 °C. (The specific value of T_{II} is not shown in this paper.)

4. UT reflection property

4.1. Outline

UT is known as a non-destructive testing technique that is generally used for detecting internal or surface defects in materials. It is assumed that the ultrasonic wave is reflected back to its source from the boundary between the zones of high acoustic impedance and low acoustic impedance. Here, acoustic impedance Z is defined as in Equation (5).

$$Z = \rho C \tag{5}$$

where C is the wave propagation speed (speed of sound) inside SiFRP, and the density (ρ) can be estimated from the TG data. It is assumed that the ultrasonic wave is reflected somewhere inside SiFRP because the acoustic impedance of SiFRP changes with the progress of the pyrolysis reactions. Thus, it becomes possible to utilize UT as a means of measuring the progress of the degraded zones of SiFRP.

The degraded thickness is easily measured after a ground-firing test of the LRE is performed and the combustor is cut into pieces. We must note here that the obtained degraded thickness represents the state after a long heat soak-back period following burnout. Indeed, according to our calculations, the progress of the charred zone ceases shortly after burnout, whereas that of the decomposed zone continues for a fairly long time.

Therefore, we have applied the UT technique to the ablative combustor in ground-firing tests of an LRE for acquiring information on the SiFRP transient thermal response data.

First, we have to determine the acoustic reflectivity (R_P) between mediums 1 and 2, which appears in Equation (6), where Z is the acoustic impedance (as defined by Equation (5)). We estimate the value of C, based on the elastic wave theory, by using the measured elastic modulus, considering the 3D orthogonal anisotropy of SiFRP.

$$R_P = \frac{Z_2 - Z_1}{Z_2 + Z_1} = \frac{\rho_2 C_2 - \rho_1 C_1}{\rho_2 C_2 + \rho_1 C_1} \tag{6}$$

For example, in the case of 1D wave propagation, the value of C will be related to the value of Young's modulus (E), as shown in Equation (7).

$$C = \sqrt{E/\rho} \tag{7}$$

Elastic modulus data for SiFRP can be obtained by several experimental methods. In this study, the forced vibration method was chosen as the primary test method, with static tension/compression tests as a backup approach. More specifically, we used Nihon Techno-Plus Corp's 'Elastic Modulus and Internal Friction Meter' (EG-HT type), whose principle is based on a resonant method with a cantilever bending and torsion mechanism. The test procedures for EG-HT are as follows:

(1) Step one: prepare a column-shaped virgin SiFRP specimen.
(2) Step two: install a vibration-generating attachment at one end of the specimen, with the other end fixed by a test rig of EG-HT.
(3) Step three: measure the normal mode vibration frequencies in both the bending and the torsional directions at specified temperatures, while increasing the specimen temperature.
(4) Step four: using the measured vibration frequencies of the normal mode value, the specimen dimensions, and the test rig properties calculate the Young's modulus and

shear modulus under an assumption of isotropy. The specimen may undergo a change of shape during heating. Because *in situ* shape change measurement cannot be performed using EG-HT equipment, we calculate the real-time shape change based on the thermal expansion date of SiFRP.

Usually, EG-HT equipment is exclusively used with materials having isotropic properties to obtain normal mode vibration frequencies in both the bending and the torsional directions, after which the Young's modulus and shear modulus are finally estimated. The Poisson's ratio can also be estimated using Equation (8).

$$G = E/\{2(1+v)\} \tag{8}$$

In contrast to the over-simplified case of 1D, actual SiFRP is assumed to have 3D orthogonal anisotropy and isotropy with regard to the X–Y plane, as shown in Figure 10. Therefore, six types of elastic coefficients, such as ($E_x(=E_y)$, E_z, G_{xy}, $G_{xz}(=G_{yz})$, v_{xy}, and v_{xz}), are required to describe its elastic motion. As shown in Figure 11, we prepared four different types of specimens that differed in the ply direction, measured the characteristic vibrations in each specimen, and then estimated inversely, using finite element method (FEM) analysis, six unknown coefficients that satisfied the vibrations. The material coordinate system is shown in Figure 10 and the schematic representation for each specimen is shown in Figure 11.

In the EG-HT equipment, test attachments were installed to enhance the bending and torsional vibrations. Thus, the obtained vibrations reflect the influence of the characteristics of the test rig. Because the test rig characteristics are not available to the public, we had to estimate the test rig properties such as its mass and inertial moment using the measured characteristic vibrations and the calculated Young's modulus and shear modulus, based on the assumption of isotropy. In this way, using the specimen model along with the estimated mass and inertial moment values, we performed characteristic vibration analysis under the assumption of 3D orthogonal anisotropy. Upon identifying the six unknown coefficients, we took advantage of the NASTRAN SOL200 optimization analysis by using the six elastic coefficients as adjustment parameters to minimize the RSS (root-sum-square) values between the computed and the measured characteristic vibration values for each specimen configuration.

The specimen shape described in Figure 11 is 40 mm × 10 mm × 2.4 mm.

4.2. *Experiments for SiFRP elastic coefficients*

The estimated values of the elastic coefficients for SiFRP obtained using the forced vibration method (EG-HT) under the assumption of 3D orthogonal anisotropy are represented by symbol I in Figure 12.

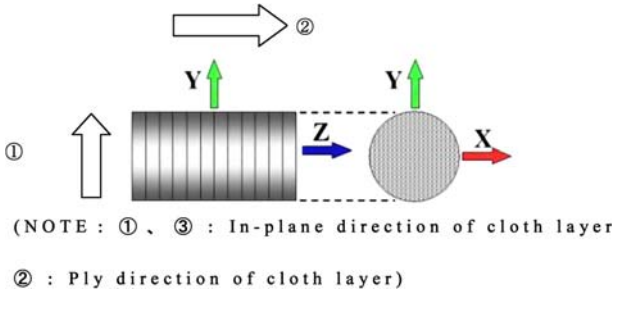

Figure 10. SiFRP material coordinate system.

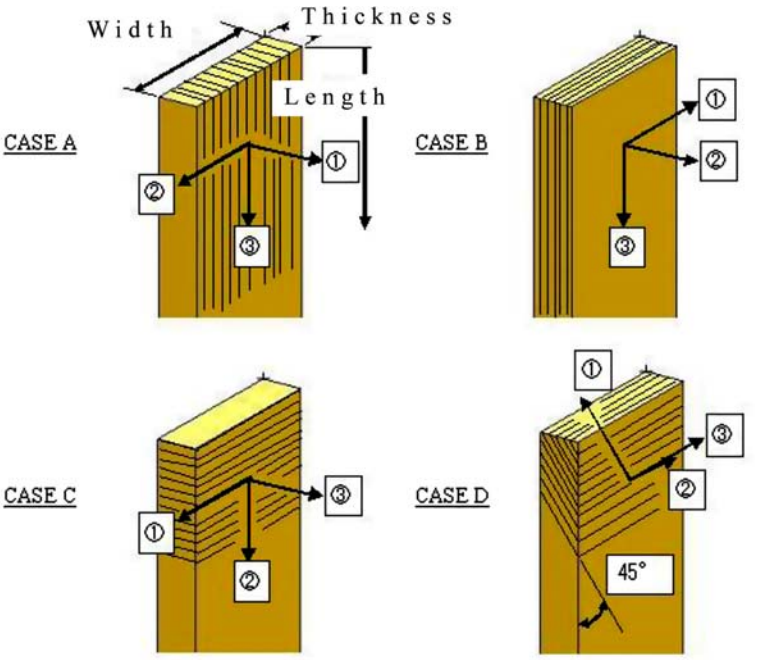

Figure 11. Illustration of tape-wrapping directions of test specimens.

In Figure 12, the measured coefficient values obtained using other experimental techniques (symbols: II-VI) are also shown. Examining the data for E_x, E_y, and E_z, we noted that the coefficient data obtained using the forced vibration method are in good agreement with the data obtained using other techniques, at least in the temperature range from room temperature to 400 °C.

4.3. *UT reflection property based on measured elastic coefficients*

As shown in Figure 10, it is assumed that SiFRP has 3D orthogonal anisotropy and isotropy with respect to the cloth-plane (X–Y plane). Therefore, the values of six types of elastic coefficients, such as $E_x(=E_y)$, E_z, G_{xy}, $G_{xz}(=G_{yz})$, ν_{xy}, and ν_{xz}, are necessary for determining the constitutive equations to predict the thermo-structural behavior of SiFRP.

Here, Hook's equation for SiFRP is described by Equation (9). For more details, please refer to reference [8]. The values of the tensors appearing in Equation (9) are expressed by the above-mentioned six types of elastic coefficients:

$$\begin{Bmatrix} \sigma_{11} \\ \sigma_{22} \\ \sigma_{33} \\ \sigma_{23} \\ \sigma_{13} \\ \sigma_{12} \end{Bmatrix} = \begin{bmatrix} C_{1111} & C_{1122} & C_{1133} & 0 & 0 & 0 \\ C_{1122} & C_{1111} & C_{1133} & 0 & 0 & 0 \\ C_{1133} & C_{1133} & C_{3333} & 0 & 0 & 0 \\ 0 & 0 & 0 & C_{2323} & 0 & 0 \\ 0 & 0 & 0 & 0 & C_{2323} & 0 \\ 0 & 0 & 0 & 0 & 0 & C_{1212} \end{bmatrix} \begin{Bmatrix} \varepsilon_{11} \\ \varepsilon_{22} \\ \varepsilon_{33} \\ \varepsilon_{23} \\ \varepsilon_{13} \\ \varepsilon_{12} \end{Bmatrix} \tag{9}$$

Based on elastic wave propagation theory, the acoustic reflectivity (R_P) defined by Equation (6) can be calculated. The estimated results are shown in Figure 13. Although the

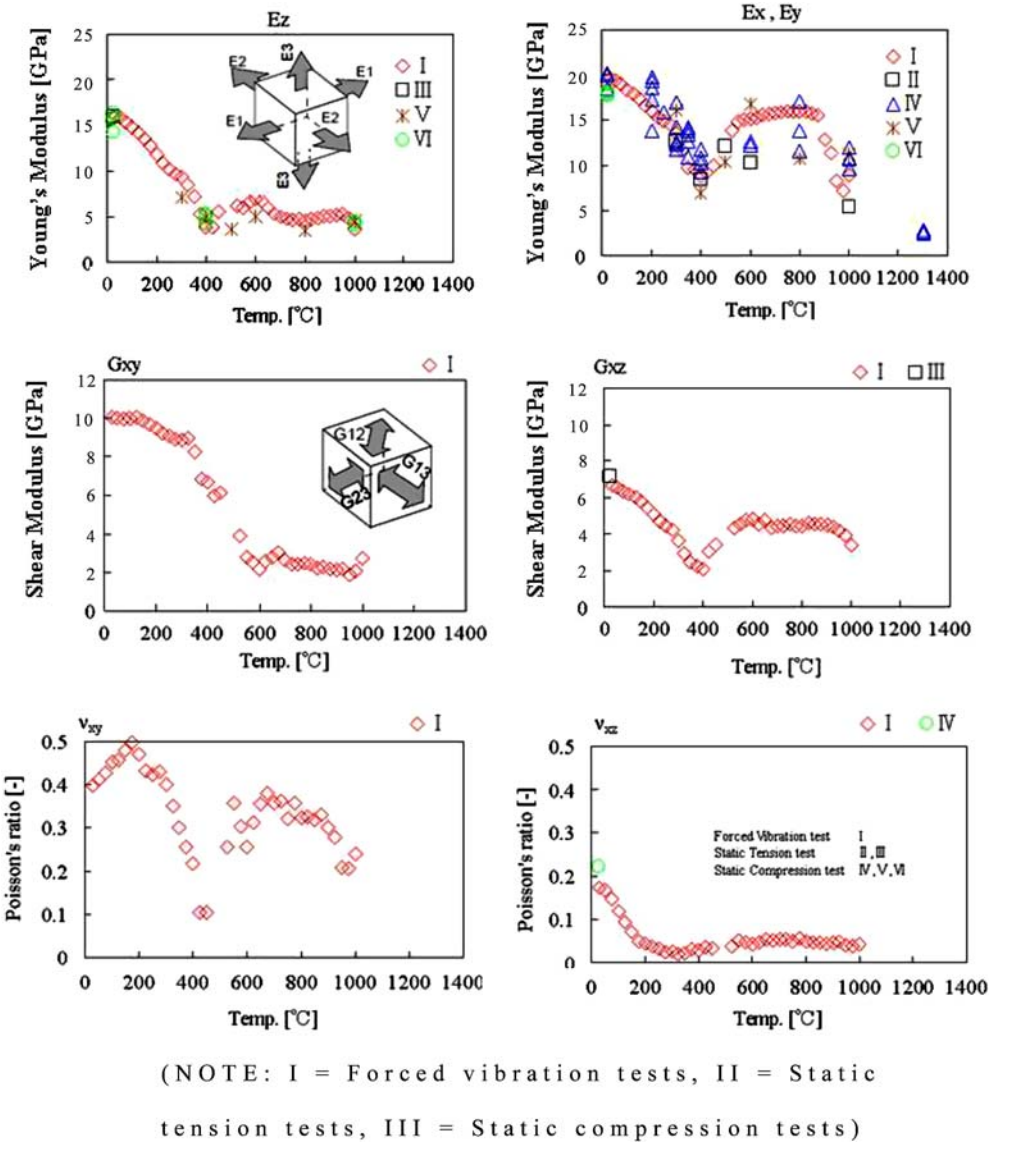

Figure 12. Estimated elastic coefficients of SiFRP.

reflection point of the ultrasonic wave is not specified in Figure 13, we have confirmed that the reflection point lies in the decomposed zone and that the acoustic reflectivity peaks at a certain temperature at around T_r.

4.4. *Validation of the assumed UT reflection property*

For validating the ultrasonic reflection point T_r, we conducted laser-heating tests by using the high-power semi-conductor laser-heating facilities of the Japan Aerospace Exploration Agency (JAXA), whose laser wavelength is approximately 1000 nm. For more details, see also reference [4].

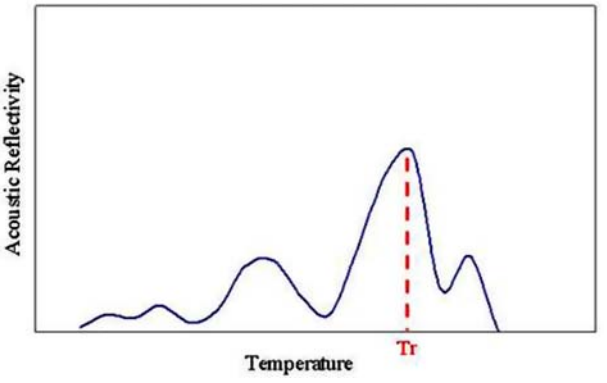

Figure 13. Estimated dependence of acoustic reflectivity of SiFRP on temperature [7].

The test specimen was a rectangular block with dimensions of $30 \times 30 \times 32$ mm, which was heated on one side under a low-pressure argon atmosphere. The specimen was fixed with two water-cooled alumina blocks with a 5-kN load to keep the blocks at approximately room temperature. Because the size of the laser beam spot was 10×10 mm, which is much smaller than the specimen size, we realized an approximately uniform heat flux on its surface using a high-speed scanning device. A UT probe was attached to the opposite side of the heated surface, and it transmitted and received ultrasonic waves during heating. In this way, a time history of the ultrasonic wave reflection point was obtained under each test condition.

On the other hand, we measured the temperature of the heated surface using a radiation thermometer and the temperatures inside the SiFRP specimen using thermocouples (dia. = 0.2 mm, type *K*). The boundary temperature between the alumina blocks and the SiFRP specimen was also measured to provide the appropriate boundary condition for numerical simulation. The duration of the laser-heating was 240 s. We confirmed that the measured temperature responses were successfully reproduced by our numerical simulation. For details of the numerical simulation, see reference [3].

The measured time histories of the ultrasonic wave reflection point during tests, the computed time histories of the degraded zone boundaries (II and III), and T_r point are shown in Figure 14.

From Figure 14, we were able to confirm that the UT measurement results and the computed T_r results are in good agreement. We were therefore able to conclude that the acoustic wave seems to be reflected at the T_r location inside the SiFRP specimen, and we can measure the real-time ablation progress using the UT technique.

5. Discussion

5.1. Characterization of I/F points inside SiFRP degraded zones

SiFRP goes through pyrolysis reactions when it is exposed to high-temperature gasses, leading to the formation of a relatively weak charred zone and decomposed zone. For this reason, two interface (I/F) points appear, namely the I/F of the charred and decomposed zones (designated as III) and the I/F of the decomposed and virgin zones (designated as II).

Based on the findings of both the TG experiments noted in Section 2 and the halogen lamp heating tests noted in Section 3, we confirmed that the extent of the pyrolysis reactions (β) at III corresponds to approximately 40% and also that the MET at II corresponds to 250 °C.

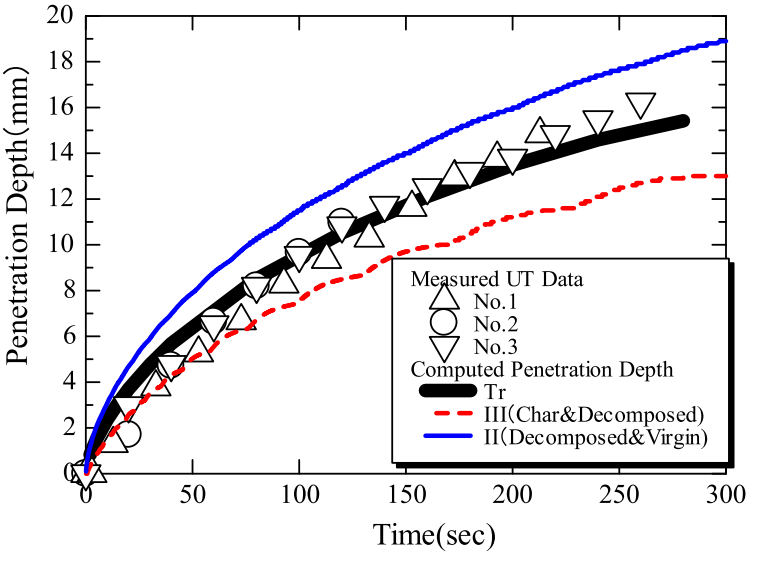

Figure 14. Comparison of measured UT (ultrasonic testing) data obtained from laser-heating test at 0.72 kW × 240 s and computed values.

5.2. *Characterization of UT reflection property inside SiFRP degraded zones*

First, based on Figure 13, which is derived from the six experimentally determined types of elastic coefficients, under the assumption of 3D orthogonal anisotropy and isotropy regarding the cloth-plane for the SiFRP specimen, we confirmed that the ultrasonic wave seems to be reflected from a certain location within the decomposed zone, and also that it is reflected approximately at a location inside the SiFRP specimen, whose temperature reaches T_r.

Second, as shown in Figure 14, we confirmed that the computed time histories of the ultrasonic wave reflection point are in good agreement with the actual UT data of the laser heating tests, assuming that the UT reflection occurs mainly at T_r .

We can therefore conclude that the UT reflection point can be approximated as T_r.

5.3. *Summary*

Based on the research presented above, we have confirmed that the observable properties that characterize SiFRP in-depth phenomena, such as

(1) Point II: the I/F of the decomposed and virgin zones.
(2) Point III: the I/F of the charred and decomposed zones.
(3) The UT reflection point.

can be successfully related to quantities that can be computed, such as the extent of the pyrolysis reaction (β) or the MET.

The primary pyrolysis reaction products of phenolic resin at relatively low temperatures are known to be H_2O, phenolic, and cresole [8]. We also conducted TG-MS (thermogravimetric mass spectrometry) studies focusing on the above three species and found that the primary product at a temperature level around T_r is H_2O.

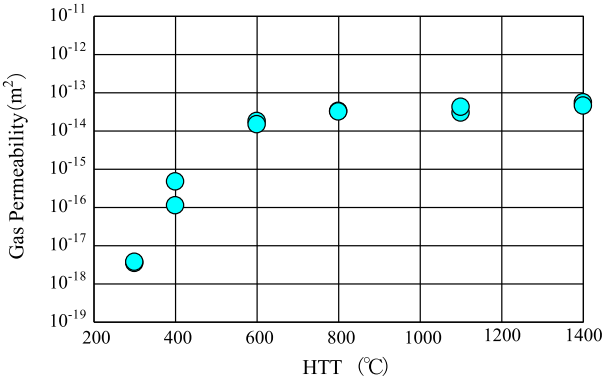

Figure 15. Dependence of SiFRP gas permeability measured at RT under N_2 gas environment on the heat treatment temperature (HTT).

According to our survey of the literature, the saturated vapor pressure of H_2O at T_r is approximately 10 MPa. As shown in Figure 15, the gas permeability of SiFRP at T_r is three orders of magnitude lower than that of perfectly charred SiFRP. Thus, this relatively slow gas motion property as compared to the generation of pyrolysis gasses inside the SiFRP specimen at T_r may lead to the formation and development of pores inside the SiFRP specimen, owing to the high-pressure H_2O vapor, and may finally maximize the UT reflection at around T_r .

With regard to this hypothesis, we believe that further investigation on the microstructure is needed to clarify the effect of the heating conditions on the resulting microstructure.

6. Conclusions

This study has focused on understanding and modeling the physical phenomena related to SiFRP in-depth phenomena, as applied to an LRE combustor. More specifically, the experimental characterization activities were divided into two areas of study:

(1) Research on the characterization of degraded zones based on TG experiments for the I/F points and laser-heating tests.
(2) Research on the UT reflection property based on the six types of elastic coefficients that were determined by forced vibration tests under the assumption of 3D orthogonal anisotropy, with isotropy regarding the cloth-plane.

Finally, these properties that were determined by basic experiments were confirmed by laser-heating tests; the purpose of this was to simulate the environmental heating conditions that are presumably encountered in an actual SiFRP combustor.

As a result of these activities, we believe that we have acquired a better understanding of SiFRP in-depth phenomena.

References

[1] Peters W, Rogers P, Lawrence T, Davis D, D'Agostino M, Brown A. Fastrac nozzle design, performance and development. AIAA-2000-3397; 2000.
[2] Judd DC, Buccella S, Alkema M, Hewitt R, McLaughlin B, Hart G, Veith E. Development testing of a LOX/methane engine for in-space propulsion. AIAA-2006-5079; 2006.
[3] Hirai K. Numerical and experimental characterizations of the SiFRP ablator for the combustion chamber heat shields of liquid rocket engines. Trans. JSASS Space Tech. Japan. 2008;7:37–42.

[4] Kinefuchi K, Kamita K, Hirai K. Study for validation of a liquid rocket engine ablative chamber (in Japanese). In: 49th Conference on Aerospace Propulsion and Power; 2009.
[5] Ho DWK, Koo JH, Bruns MC, Ezekoye OA. A review of numerical and experimental characterization of thermal protection materials – Part III. Experimental testing. AIAA-2007-5773; 2007.
[6] Hirai K, Matsuura Y, Kinefuchi K, Kamita T. Experimental investigations on the thermo-chemical phenomena in SiFRP. J. Jpn. Soc. Compos. Mater. 2012;38:228–235. Japanese.
[7] Matsuura Y, Hirai K. A challenge of predicting thermo-mechanical behavior of ablating SiFRP with finite element analysis. In: 46th AIAA/ASME Joint Propulsion Conference, AIAA-2010-6975; 2010.
[8] Trick KA, Saliba TE. Mechanisms of the pyrolysis of phenolic resin in a carbon/phenolic composite. Carbon. 1995;33:1509–1515.